Building a Mycenaean chamber tomb catalogue from terrestrial laser scan data

Gutierrez, Ivan; Lindenbergh, Roderik; Watson, Lisa; Shelton, Kim

DOI
10.1016/j.daach.2024.e00319

Publication date
2024

Document Version
Final published version

Published in
Digital Applications in Archaeology and Cultural Heritage

Citation (APA)
Gutierrez, I., Lindenbergh, R., Watson, L., & Shelton, K. (2024). Building a Mycenaean chamber tomb catalogue from terrestrial laser scan data. *Digital Applications in Archaeology and Cultural Heritage*, *32*, Article e00319. https://doi.org/10.1016/j.daach.2024.e00319

Digital Applications in Archaeology and Cultural Heritage 32 (2024) e00319

Contents lists available at ScienceDirect

Digital Applications in Archaeology and Cultural Heritage

journal homepage: www.elsevier.com/locate/daach

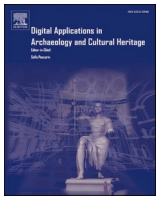

Building a Mycenaean chamber tomb catalogue from terrestrial laser scan data

Ivan Gutierrez [a,*], Roderik Lindenbergh [b], Lisa Watson [a], Kim Shelton [c]

[a] Department of Energy Resources, University of Stavanger, Norway
[b] Department of Geoscience and Remote Sensing, Delft University of Technology, the Netherlands
[c] Nemea Center for Classical Archaeology, Department of Ancient Greek and Roman Studies, University of California Berkeley, USA

ARTICLE INFO

Keywords:
Tombs
Mycenaean
Terrestrial laser scanning
Catalogue
Segmentation
Digital documentation

ABSTRACT

Detailed 3D information on vulnerable archaeological sites can document cultural heritage and contribute to its preservation. The Late Bronze Age Mycenaean cemetery of Aidonia, Greece, is a representative case of a vulnerable site. Tomb looting has occurred sporadically since the 1970s, when the Greek government was made aware of the site. Anthropogenic activities and natural denudation may affect the loss of structural integrity of tombs. In this contribution, terrestrial laser scanning and geosciences are combined to document the vulnerable cemetery through the generation of a tomb catalogue. The emphasis is on techniques applied to point clouds to extract architectural elements. The catalogue consists of 208 architectural and geological measurements, 112 qualitative observations, maps, and point clouds images displaying the architecture of 16 tombs. The tombs are mainly orientated northeast-southwest and northwest-southeast, and their average total length is 13 m. The average volume of chambers with preserved roofs is 46 m3.

1. Introduction

Mycenaean settlement remnants primarily exist in present-day Greece and western Turkey, dating back to the Late Bronze Age (LBA; *ca.* 1650-1065 BCE) (Cline, 2010). As of 2004, 378 Mycenaean settlement sites were reported in the Peloponnese (Wright, 2004). Funerary evidence collected through systematic excavations in tombs has improved the understanding of funerary cultural practices and social structure (Cavanagh and Mee, 1998; Shelton, 2020). LBA Mycenaean tomb types include pits, cists, shafts, built graves, tholos and tholoids, and chamber tombs (Cavanagh and Mee, 1998; Galanakis, 2018). The chamber tomb is the most common architecture found in Greece and western Turkey, where ca. 4000 specimens have been reported since the 1860s (Galanakis, 2018). Chamber tombs are cut into hillsides or soft rock outcrops. A typical chamber tomb consists of three major architectural elements: i) an entrance passage (dromos, pl. dromoi) that is dug from the ground surface at an angle towards the doorway of the chamber, creating a wedge-like shape; the width of the passage widens from surface to doorway; ii) a doorway (stomion, pl. stomia) to the chamber; and iii) the underground burial chamber (thalamos, pl. thalamoi) (Karkanas et al., 2012).

Cemetery surveying and tomb cataloguing play an essential role in funeral archaeology as tools for exploration and documentation, and contribute to the protection of burial sites under threat of natural and anthropogenic processes (Weeks, 2010). Regarding Mycenaean cemeteries, few catalogues and surveys have been published. In their comprehensive catalogue, Cavanagh and Mee (1998) reported upon 179 LBA cemeteries in mainland Greece. The chamber tomb is the most common type of architecture in these cemeteries. The catalogue is organised chronologically and geographically. The sites are shown methodically on maps. Analogue drawings depicting the architecture and distribution of tombs within cemeteries are provided for some of the sites. Galanakis (2018) provides an update on the LBA cemetery inventory by including known sites and new discoveries reported in the central and southern Aegean since 1993. According to the survey, ca. 1700 LBA tombs, which correspond to ca. 27% of the total LBA tombs discovered since the 1860s, have been marked in 207 cemeteries since the early 1990s. With 809 tombs reported in 124 cemeteries, the chamber tomb is the dominant type of architecture. The survey only provides maps showing the location of the sites.

With such extensive site inventories published, effort must focus on generating digital catalogues to permanently document the architectural features of reported tombs and cemeteries with high accuracy and precision. The success of digital tomb cataloguing may depend on the

* Corresponding author.
E-mail address: ivan.gutierrez@uis.no (I. Gutierrez).

https://doi.org/10.1016/j.daach.2024.e00319
Received 2 July 2022; Received in revised form 21 December 2023; Accepted 24 January 2024
Available online 10 February 2024

broad implementation of methods and techniques that speed up the collection and documentation of archaeological excavation data. Optical mapping methods, notably photogrammetry and laser scanning, enable a faster, high-resolution, and objective depiction of archaeological sites through non-invasive collection of accurate and precise 3D data (Remondino and El-Hakim, 2006; Böhler and Marbs, 2002; Lambers and Remondino, 2008). These optical methods have proven to be efficient in archaeological research at regional, local, and object scale (Lambers and Remondino, 2008; Remondino, 2011).

There is a progression in tomb cataloguing, from analogue (Slane, 2017) to digital (Mozas-Calvache et al., 2023; Pérez-García et al., 2019). Turner (2020) combined photogrammetry and total station to generate highly accurate models of 86 LBA Mycenaean tombs located in cemeteries in Menidi, Portes and Voudeni, in mainland Greece, where chamber tomb structures are the most common type. The catalogue includes orthophoto mosaics, maps showing the location of the tombs, visualisations of the 3D photogrammetric models, and a table with 12 variables listing the architectural dimensions of the tombs, including volume, height, width, and length. However, previous Mycenaean cemetery catalogues do not incorporate terrestrial laser scanning (TLS). TLS is a highly accurate and non-invasive method that is fairly rapid in collection time (Vosselman and Maas, 2010). TLS allows capturing the cemetery's layout at local (architectural elements of the chamber tombs and the terrain's morphology above) and object scale (mesoscopic features on the surface of the architectural elements). Unlike passive sensors such as cameras, TLS is not light-dependent and is well suited for collecting data inside chambers, where photogrammetry is not an optimal solution in poor lighting conditions.

The LBA Mycenaean cemetery of Aidonia, Greece, is a representative case of a vulnerable archaeological site. Any plans to preserve it must be based on detailed studies of its present structural integrity. Digital cataloguing using TLS assists archaeologists, curators, and authorities in making informed decisions regarding long-term preservation strategies. This contribution combines geomatic and structural geology to generate a digital catalogue of the Aidonia cemetery using TLS technique. The focus is on the methodology implemented to generate the catalogue. This study aims to:

- Contribute to heritage protection of the LBA cemeteries in the region.
- Promote best practices for the preservation of the Aidonia cemetery; provide education and outreach to scientific communities and government authorities; and promote tourism.
- Advocate for substituting paper-based archaeological cataloguing with mapping optical techniques, such as TLS, integrated with other geoscientific disciplines.
- Provide a better 3D understanding of the architecture and layout of the LBA tombs in the Aidonia cemetery.
- Contribute to future studies focused on the exploration of undiscovered tombs in the Aidonia Cemetery.

The general objective of this study is to generate a digital and graphic catalogue to permanently document, on a local scale, the Mycenaean cemetery of Aidonia. In order to accomplish the objective, this study focused on answering the following research question: Can the TLS technique combined with geosciences be applied to generate a digital and graphic catalogue that documents in 3D and high detail the architectural aspects and topographic setting of the Aidonia cemetery?

After introducing the Aidonia cemetery (Sub-section 1.1), the methodology (Section 2) describes in detail the used tomb segmentation method. Subsequently, the resulting tomb catalogue is presented (Section 3) together with a general description of the cemetery setting and the tombs, whose location, layout, and structural integrity are used as correlation and grouping criteria. The advantages and challenges of the techniques used are discussed (Section 4), followed by conclusions and recommendations (Section 5). Archaeological interpretations go beyond the scope of this study.

The complete graphic catalogue is available in the supplementary material. The TLS raw point clouds are published at https://data.4tu.nl/ (doi: 10.4121/df349dfc-9668-4169-a7d6-9852d68b4adf.v1). Videos 1 nd 2 enclosed with the electronic version of this article show the external and internal structure of tomb 9. The point cloud shown in the videos was thinned to a 0.05 m point spacing.

1.1. The Mycenaean cemetery of Aidonia

In the northeastern Peloponnese, a Mycenaean cemetery is located in present-day Aidonia, Greece, on a hillside on the western flank of the Phlious basin (Fuchs et al., 2004; Casselmann et al., 2004) (Fig. 1). Although Aidonia cemetery is reported among the mortuary sites in the Peloponnese by Cavanagh and Mee (1998) and Galanakis (2018), very little additional information is published. The chamber tombs of the Mycenaean cemetery of Aidonia were dug within soft layers of marls of the Member B of the Upper Pliocene Psari Formation (I.G.S.R, 1970; Paraskevopoulos, 1990; Fuchs et al., 2004). The cemetery is currently divided into three parts: lower, middle, and upper (Kvapil and Shelton, 2019). Intensive looting in the middle cemetery was reported in 1977 before official rescue excavations by the Greek Archaeological Service began in 1978 (Krystalli-Votsi, 1998; Krystalli-Votsi and Kaza-Papageorgiou, 2013).

Originally, the middle cemetery consisted of 20 tripartite (dromos, stomion, and chamber) tombs and tomb-related features (Krystalli-Votsi and Kaza-Papageorgiou, 2013): sixteen tombs with chambers (1–11, 15–17, 19, 20), one vertical shaft (12), two dromoi without chambers (13 and 14), and one small chamber cist (18). The structures contain rich Mycenaean burials comparable to those found at the Mycenae and Dendra cemeteries in Argolid (Demakopoulou, 1998b). Some of the burials are found in pits dug in the chamber floor; others are found around the deceased on the chamber floor and niches dug in the dromoi and chamber walls. In general, human and horse remains and pottery date the tombs to the Late Helladic IIIA2 and IIIB periods (ca. 1350 BCA) (Kaza-Papageorgiou, 1998). Some burials contain weaponry, gold, and jewellery (Touchais, 1987; Krystalli-Votsi, 1989; Demakopoulou, 1998a; Shelton, 2020). The archaeological richness and architecture of the tombs in Aidonia suggest a high level of wealth in Mycenaean society that inhabited the region (Shelton, 2020). Unfortunately, 13 tombs were heavily looted while two were illegally excavated but not looted. Only five tombs remained untouched after illicit digging activities in the 1970s and 1980s (Krystalli-Votsi and Kaza-Papageorgiou, 2013). Additionally, the tombs have undergone notable degradation. Some tombs have roofs completely collapsed due to the loss of structural integrity of the natural rock formation. We believe that natural denudation and anthropogenic activities, including agriculture and looting, are the main processes that have hampered the preservation of the tombs. Since 2014, exploration campaigns and systematic excavations have been carried out by the Korinthian Ephorate of Antiquities and the Nemea Center for Classical Archaeology (TAPHOS-Tombs of Aidonia Preservation, Heritage, exploration, Synergasia) in order to preserve the architecture of the tombs and the remaining cultural artefacts in the Aidonia cemetery (Shelton, 2020).

2. Material and methods

The implemented methodology comprises five main steps (Fig. 2): i) Acquisition of TLS data (Section 2.1); ii) Pre-processing of point cloud (Section 2.1); iii) Unwanted object removal (Section 2.2); iv) Tomb segmentation (Section 2.3); and v) Tomb cataloguing (Section 2.4).

2.1. TLS data acquisition and pre-processing

Laser scanning, Fig. 2, was carried out in August 2019 with a Leica ScanStation C10 (Leica Geosystems, 2021), scanning the sloped terrain of the cemetery and 16 chamber tombs. 51 scan positions make up the

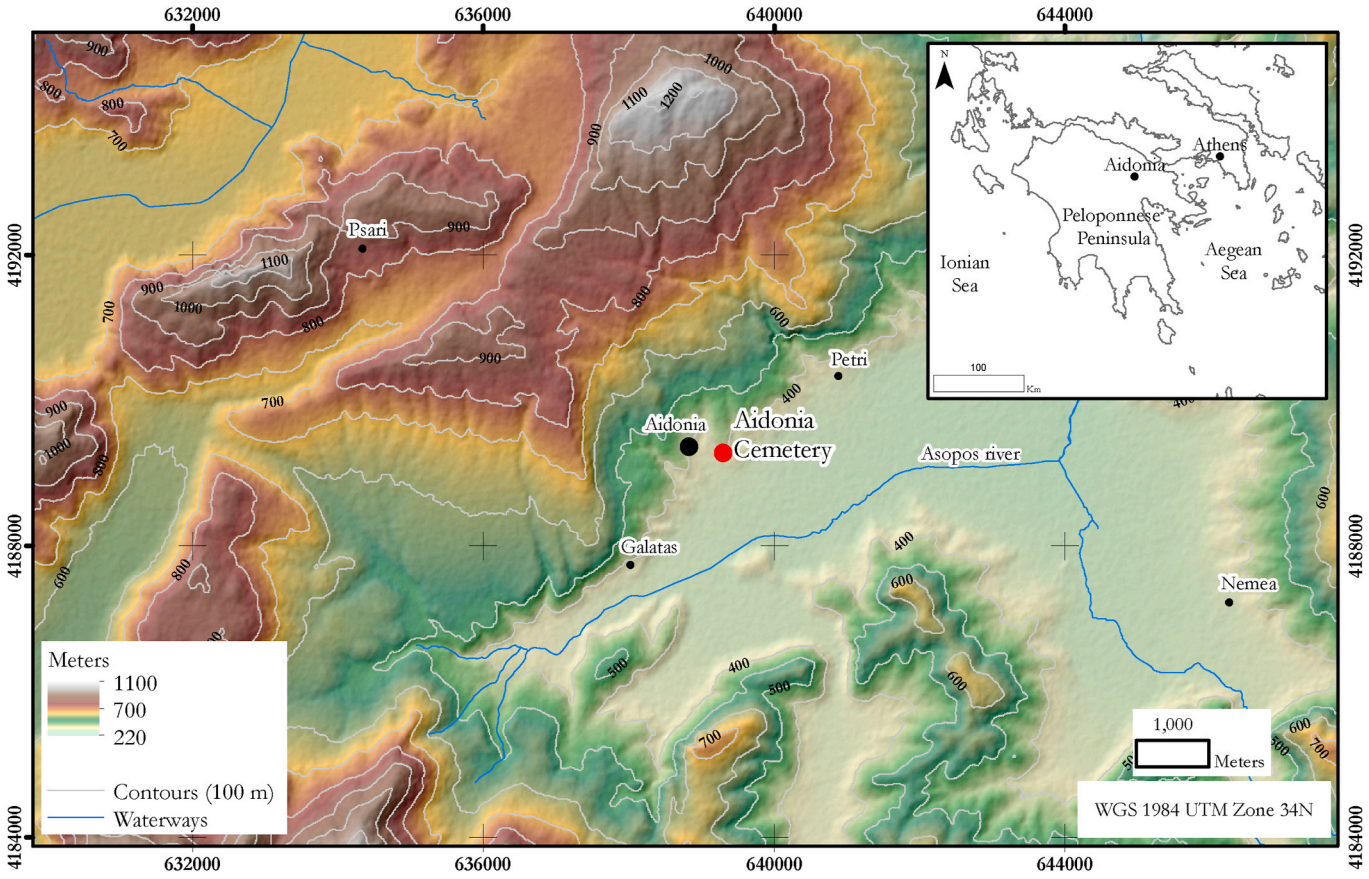

Fig. 1. Location of the Aidonia cemetery ca. 385 m above sea level at the foothills of the Asopos river valley. ALOS PALSAR - radiometrically terrain corrected (RTC) digital elevation model (DEM) (ASF DAAC, 2015; Logan and Coauthors, 2014). The location of the Aidonia village within Greece is shown on the inset map.

TLS campaign, of which 29 positions focus on the dromoi and chambers, and 22 positions on the cemetery setting. All scan positions were registered in a local coordinate system using targets, yielding an average error of 0.005 m. With a laser beam footprint of 7 mm; the scanner delivers a point spacing of ~3 mm at a distance of 10 m, while point spacing decreases to ~0.7 mm at short scan distances employed inside chambers and dromoi. The acquired point clouds contain ~ 5.9 billion points. Features associated with individual points consist of three spatial coordinates (x, y, z) and intensity. Fig. 3 displays the raw point clouds for tomb 9 and the terrain above it. The characteristics of the terrain and the tomb entrances can be seen together with other terrain objects (e.g., vegetation; Fig. 3b). The main architectural elements of the tombs (chamber, stomion and dromos) and additional features such as mortuary pits in the chamber were also captured (Fig. 3c, top).

Due to the size of the raw point clouds, data processing is computationally expensive. Noise and outliers were removed in the pre-processing steps, which comprise outlier removal, 3D data thinning, and georeferencing (Fig. 2). Points with less than ten neighbours within a radius of 0.1 m were considered outliers and removed. 3D block thinning was performed to preserve only those points nearest to the centre of voxel units with an edge length of 0.05 m. Subsequently, a georeferenced TLS dataset acquired in July 2017 as a pilot study in the middle cemetery was used as reference for positioning the 2019 point clouds in the WGS84 global coordinate system with projection UTM Zone 34 North. To do so, the Iterative Closest Point algorithm (ICP; Besl and McKay, 1992) was used to match corresponding stable planar surfaces extracted from dromoi walls scanned in both 2017 and 2019. The 2017 scan positions were collected with a differential GNSS of centimetre accuracy. Pre-processing steps, as well as the upcoming steps of the workflow, were implemented in CloudCompare (Girardeau-Montaut, D., 2016) and in the proprietary add-on LIS Pro 3D (Laserdata, 2017) that operates within the SAGA platform environment (Conrad and Coauthors, 2015).

2.2. *Unwanted object removal*

Removal of unwanted objects consists of identifying and removing points corresponding to vegetation and any other objects, such as scan targets, tripods, and people (Fig. 3). As a result, only points representing chamber tombs and terrain are kept. Separating vegetation and objects from tombs and terrain is a challenge. The scanned scene is complex; it is on a slope and combines the heterogeneities of the natural terrain on the surface with simpler anthropogenic underground structures. In this case, terrain extraction is a 3D problem that cannot be adequately solved with traditional ground filtering techniques (e.g., Axelsson, 2000; Zhang et al., 2016; Evans and Hudak, 2007) designed for airborne laser scanning. The method proposed by Brodu and Lague (2012) was tailored to the complex scene of Aidonia cemetery. The method uses multi-scale dimensionality criteria to classify objects in complex environments. It geometrically characterises 3D point clouds at different scales by semi-supervised machine learning, where representative training samples were manually extracted to train a classifier. The samples were grouped into two classes: tomb/terrain and unwanted object.

The sample classes exhibit a wide range of scales. The unwanted object class includes vegetation such as short grass (≈0.15 m), bushes (≈0.4 m), and trees (≈5 m–8 m). In contrast, the tomb/terrain class includes dromoi that range from 2 m to ~10 m in length. The classifier was generated using training samples on 150 scales between 0.1 and 15 m with a step of 0.1 m. The classifier separated the two training classes with an accuracy of 98%. Subsequently, the classifier was applied to the full dataset. Points classified as unwanted were removed. Fig. 4 illustrates the classification of unwanted points that correspond to grass on

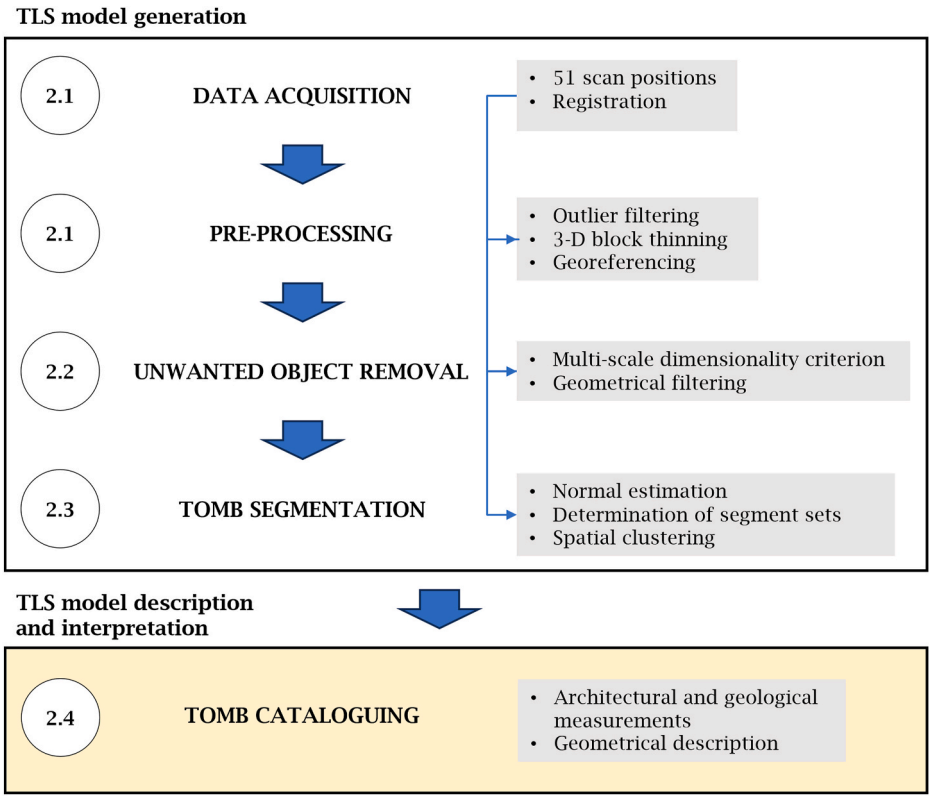

Fig. 2. Illustration of the implemented methodology. Steps depicted in the workflow are aligned with the sub-sections contained within this section, as denoted by respective numerical labels.

top of tomb 9. After the removal of most unwanted objects, small groups of misclassified points remained. The geometric point features (Weinmann et al., 2017) surface density and planarity were computed and sufficient to remove unwanted remnant points.

2.3. *Tomb segmentation*

Tomb segmentation consists of subdividing the chamber tombs into architectural elements such as doors, walls, roofs and floors. This enables analysing geometrical characteristics of each tomb element. Tomb segmentation was achieved using point features to group clusters of points (i.e., segments) that share similar characteristics (Nguyen and Le, 2013; Vosselman, 2013). For example, points that fit into the same plane are merged if they are spatially close and share local point features (Vosselman and Maas, 2010).

Tomb surfaces hewn by Mycenaeans in the natural rock formation can be thought of as joint planes exhibiting different orientations, which are described by geological measurements such as dip direction and dip angles. The dip direction indicates towards which direction a plane is dipping. It is 90° off the azimuth, which corresponds to the horizontal angle (measured clockwise from the north) of the intersection line of an inclined plane and a horizontal plane (Ragan, 2009). The dip is the steepest vertical angle (0° - 90°) of an inclined plane relative to a horizontal plane. The method of Wichmann et al. (2019) intends to automatically derive joint orientations and joint set clustering from TLS point clouds, as well as to determine joint normal spacing and the distribution of *in situ* block sizes. The method suits well for tombs exhibiting planar to fairly planar surfaces (tombs 2–4, 6–11, 15, and 19). To apply this method, the chamber and dromos of each tomb were manually split beforehand. The process for segmenting tomb 9 is illustrated in Fig. 5. Three main steps were required (Fig. 2; 2.3):

1. Normal estimation: The RANdom SAmple Consensus algorithm (RANSAC; Bolles and Fischler, 1981) is employed to estimate a normal vector for each point from a best-fit plane containing at least six points from its 25 nearest neighbours. The plane is used as a seed for surface growing (Besl and Jain, 1988; Sapidis and Besl, 1995; Vieira and Shimada, 2005), which groups spatially connected points whenever the difference between the angles of the normals is not above a predefined value. Since the planarity of tomb surfaces ranges from planar, fairly planar to poorly planar, it is likely to obtain normal vectors pointing in opposite directions within the same surface. Therefore, lax parameters were set to better represent the smoothness of the surfaces. However, lax parameterisation varies from one tomb to another, as each tomb exhibits its own morphological heterogeneity.
2. The determination of segment sets is executed in two phases:

Generation of density pole plots: The objective is to visualise direction domains representing the segments (e.g., the back wall of a chamber). The orientations of poles are plotted in a stereonet (Groshong, 2006). The output is a density grid containing the number of poles per pixel (Fig. 5a; top left). Quadratic kernel density estimation (KDE) is performed to determine the clusters of poles with similar orientation within a radius of 10° on the diagram. The highest density values are depicted by the darkest pixels located in the centre of the faded circles (clusters of largest segments). Seven principal poles representing the orientation of the largest segments (i.e., back, front, and lateral walls, floor, and roof pitches) of tomb chamber 9 are plotted in the stereonet of Fig. 5a (top left).

Ranking and grouping of segments: The segments are ranked from highest to lowest based on their KDE values and grouped into five sets representing the five main orientations. Subsequently, an identifier (ID, from 1 to 5) is assigned to each set (Fig. 5a). The segment sets are grouped if the acute angle between their poles is less than the minimum

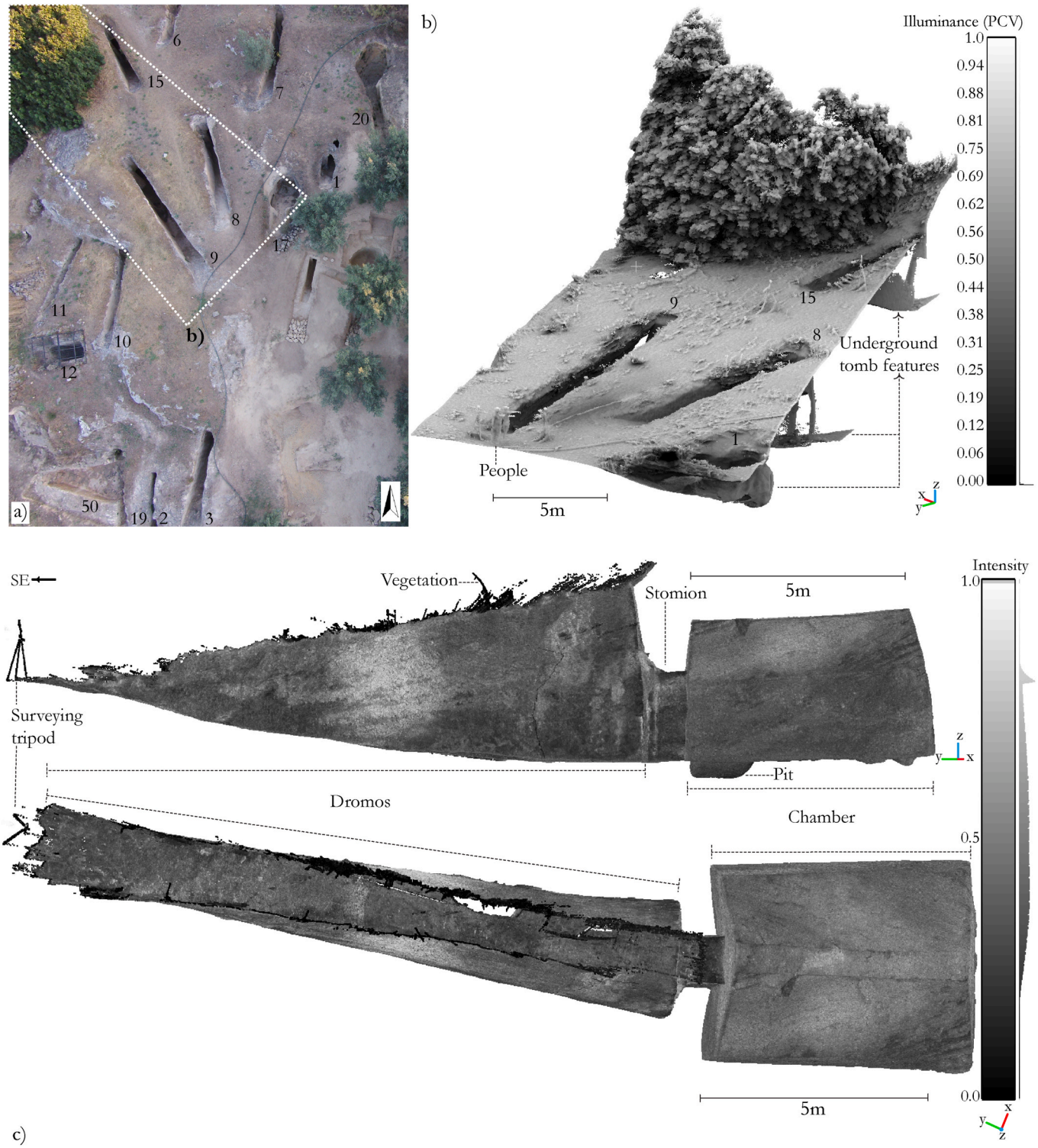

Fig. 3. Top-down view of the Aidonia cemetery and example of TLS raw point clouds. a) Aerial digital imagery collected by drone (Courtesy: Nemea Center for Classical Archaeology, 2019). Tombs and other archaeological features are numbered. b) Perspective view of part the cemetery; location is depicted by the dotted line in a. Point cloud visualization using calculated illuminance (Tarini et al., 2003). Note the morphological features of the terrain and the objects on top and underground. c) side and top-down views of chamber tomb 9 illustrating the three major elements (chamber, stomion, and dromos). Raw point cloud with point spacing of ca. 0.7 mm displayed using intensity attribute.

required between two different sets. This is the case for those sets that are almost parallel to each other. Segment set IDs are assigned to each point if the acute angle between the point normal and the normal of a pole's set does not exceed a preset angle threshold.

3. Spatial clustering separation: Finally, the segment sets representing the five principal orientations are partitioned into individual segments. This is achieved by employing the region-growing algorithm constrained by the segment set IDs to separate surfaces with the same orientation but with no spatial connection. As a result, the point

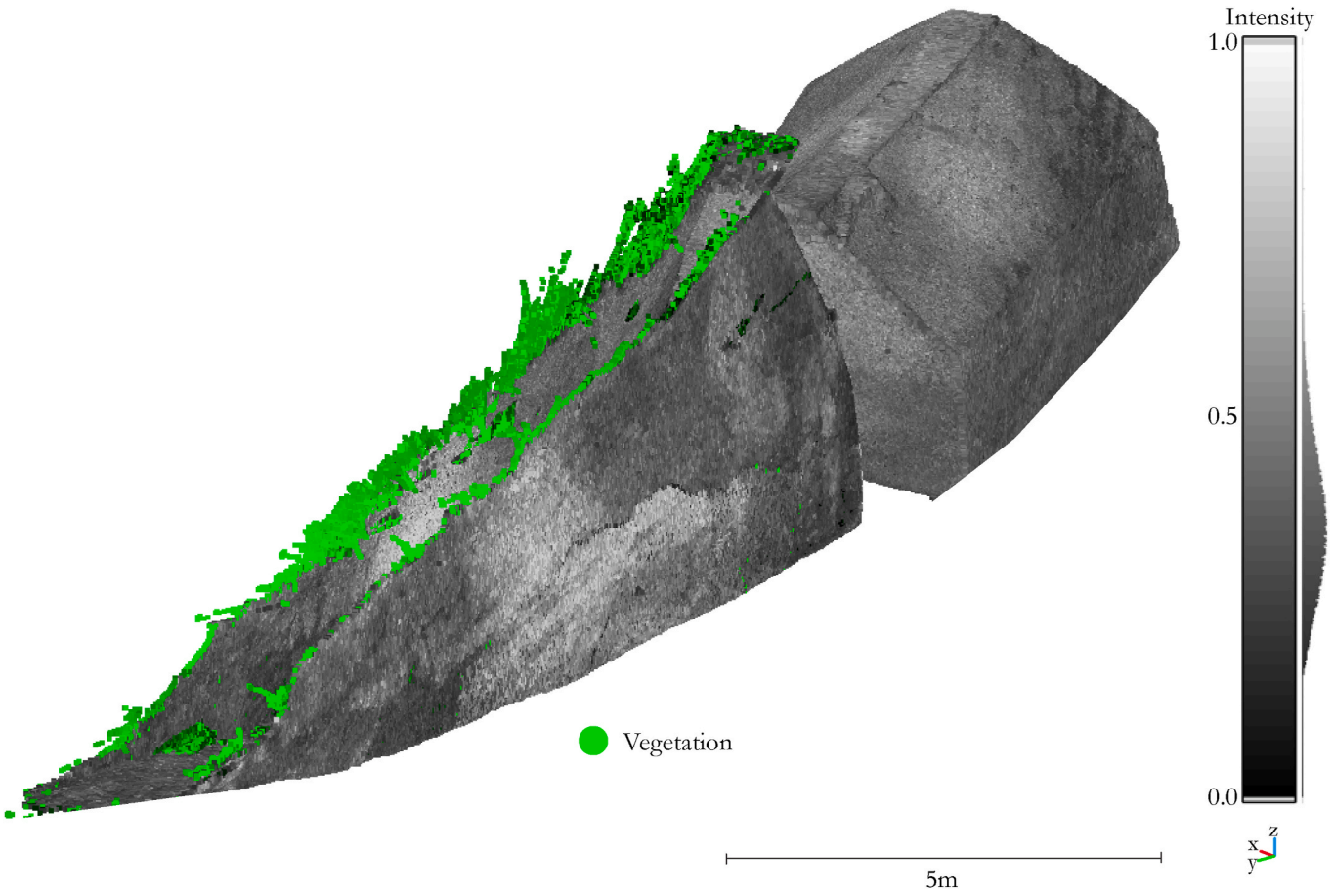

Fig. 4. Perspective view of tomb 9 showing the detection and classification of grass (artificially coloured green) along the top edge of the dromos using the multi-scale dimensionality criterion method (Brodu and Lague, 2012). (For interpretation of the references to colour in this figure legend, the reader is referred to the Web version of this article.)

cloud of the chamber of tomb 9 is partitioned into 13 different segments representing the tomb's main architectural elements (Fig. 5b).

For tombs (1, 5, 16, 17, and 20) exhibiting rounded or poorly planar geometries, the segmentation process was performed manually. Fig. 6 illustrates the process for tomb 1. First, after deriving normal vectors, the dip angle attribute is estimated for each point using a local best-fit plane constructed from neighbouring points within a radius of 10 cm (Fig. 6a). Second, the chamber is manually separated from the dromos. Third, sub-horizontal surfaces of the chamber are extracted from the cloud. Finally, the remaining points representing chamber walls are segmented by manually clipping the point cloud at high curvature areas (Fig. 6b).

2.4. *Chamber tombs measurements and qualitative criteria*

Once the chamber tombs were segmented, the orientations and dimensions of the main architectural elements were obtained. Architectural and geological measurements of the segmented point clouds (Table 1) were taken in the dromos, the stomion, and the chamber. Surface orientations were obtained by measuring dip-direction and dip angles of their best-fit plane representation. The length, width, and height of the chamber were measured directly on the clouds passing through the chamber centroid. The chamber area was measured at the base polygon that contains most of the chamber floor points. The polygon belongs to a set of polygons that envelope horizontal slices of points obtained by vertically dissecting the clouds every 10 cm. The local dip angle of the terrain above the tombs was computed directly on the terrain point cloud. Subsequently, the acute angle between the floor of the dromos and the terrain was measured using a script in MatLab (Cardozo in Allmendinger et al., 2011).

A triangle mesh representation was used to estimate the volume of each chamber. The Poisson surface reconstruction algorithm (Kazhdan et al., 2006) is well suited to reconstruct meshes representing closed 3D shapes. Except for those missing the roof, chambers are mostly closed 3D shapes. Therefore, the reconstruction delivers feasible meshes that honour the point clouds in most of the tombs. Note that due to the absence of points, there is a high degree of extrapolation in the area of the stomion (Fig. 7).

Qualitative criteria (Fig. 2; 2.4) help describe the geometry and the current structural condition of chambers and dromoi from visual observations made in the point clouds. The following criteria were used:

Overburden integrity: This criterion describes the degree of preservation of the tombs based on visual assessment of the structural integrity of the chamber overburden. In this study, the overburden of a chamber is defined as the thickness of the rock formation from the ceiling of the chamber to the surface of the terrain (Fig. 8 a). The structural integrity of the chamber's overburden is described in three categories (Fig. 8a): i) continuous: even if pieces of the overburden have fallen and fractures are present, the overburden is still continuous above the whole chamber; ii) partially-collapsed: pieces of the overburden have fallen to the point that the roof is not continuous (presence of holes), although it still covers most of the chamber; and iii) collapsed: no overburden at all.

Dromos' walls integrity: Three categories are defined to describe the degree of preservation of the dromoi based on the degree of

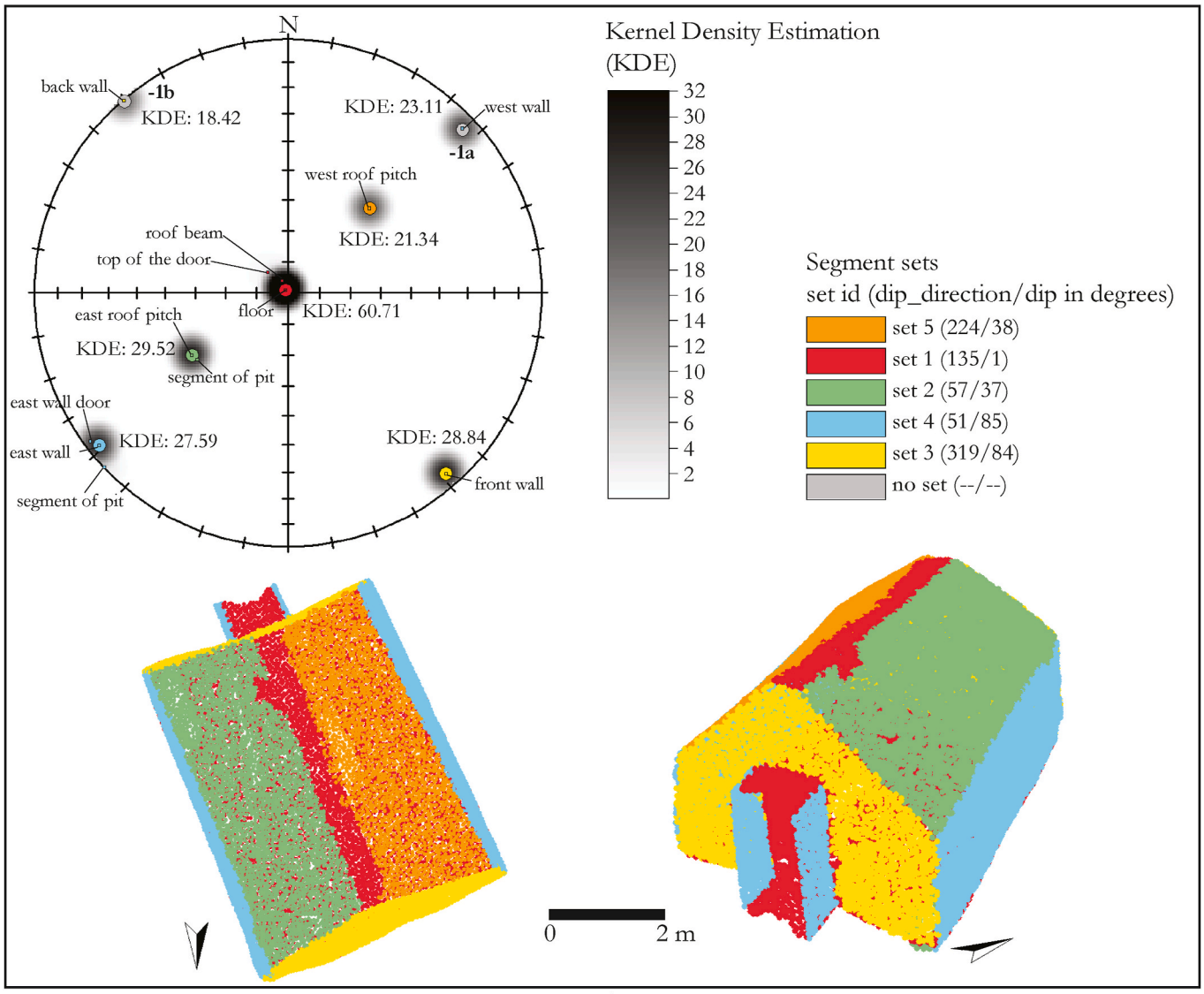

a)

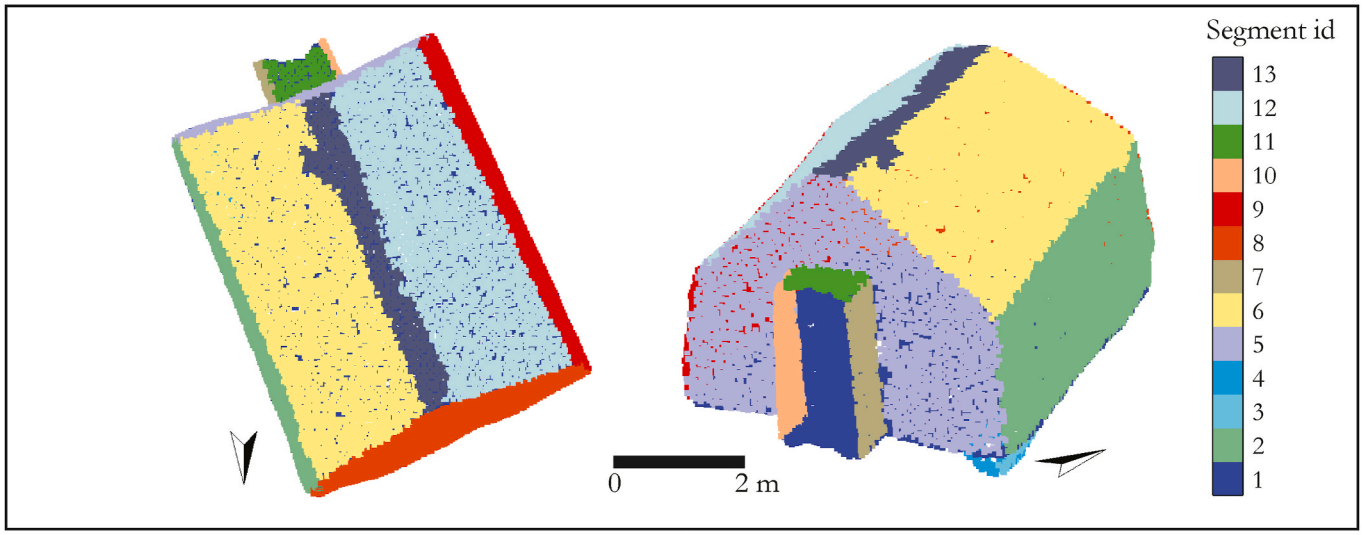

b)

Fig. 5. Segmentation of the chamber of tomb 9. a) Determination of segment sets. Top: Poles to planes of principal clusters plotted in a stereonet. Bottom: top-down (left) and perspective (right) views of the point cloud coloured by segment sets id. b) Partition into individual segments. Top-down (left) and perspective (right) views of the point cloud coloured by segment id.

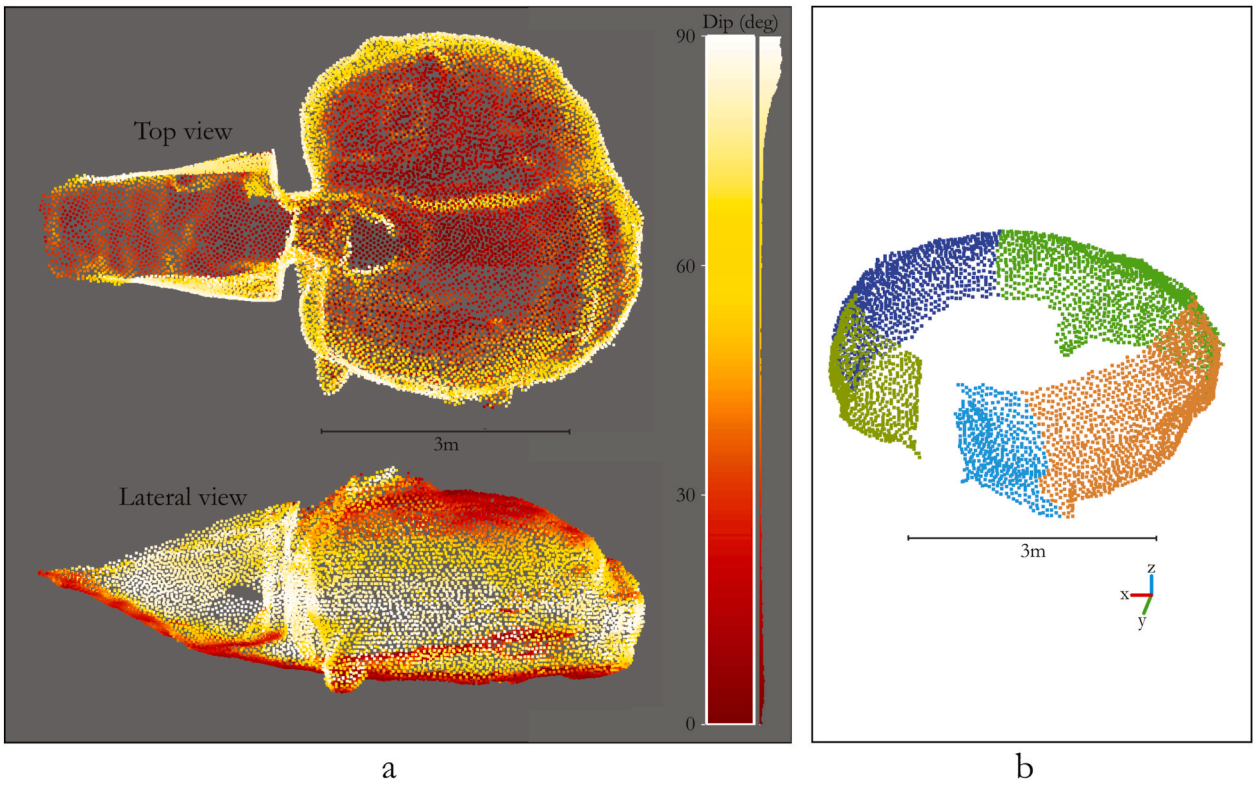

Fig. 6. Manual segmentation of tomb 1. a) Top-down and side views of the point cloud coloured by dip angle. b) Perspective view illustrating the manual segmentation of the chamber walls after extracting the chamber roof and floor using the dip angle attribute.

Table 1
Types of measurements of major architectural elements. Dip direction and dip angles are given in degrees; length, width, and height in meters; and area and volume in square meters and cubic meters, respectively.

Structure	Architectural Element	Measurement
Dromos	Lateral walls	Dip-direction and dip
	Floor	Dip-direction and dip; Length
Stomion	Façade	Height
Chamber	Lateral walls	Dip-direction and dip
	Floor	Area
	Chamber	Length; Width; Height; Volume

irregularity observed in the walls and the walls' lateral and vertical continuity: i) well-preserved; ii) fairly-preserved; and iii) poorly-preserved.

Ceiling type: Qualitative criterion aimed to describe the type of chamber ceiling observed in the point clouds. Four categories are defined (Fig. 8b): i) domed; ii) gabled; iii) vaulted (gabled with a horizontal beam between the two pitches); and iv) flat. Note that due to the integrity of the present-day overburden, the assigned ceiling type might not correspond to the original one.

Shape: Qualitative criterion to define the shape of the chamber depicted by a horizontal slice of a point cloud. The horizontal slice outlines the chamber at the height of the sensor. Chambers can be classified as: i) circular; ii) semi-circular; iii) polygonal; and iv) semi-

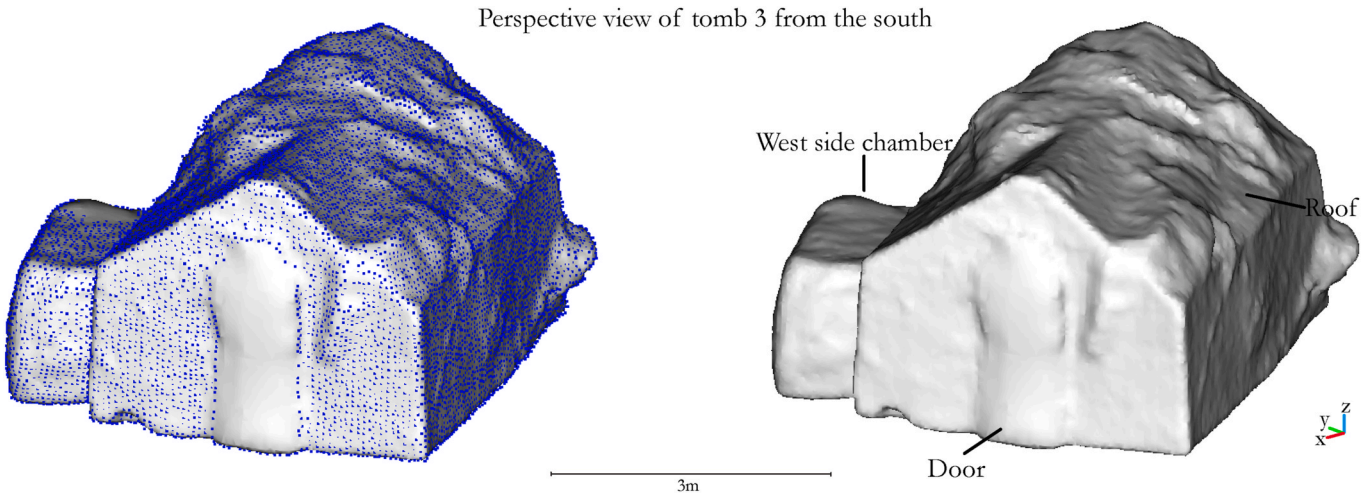

Fig. 7. 3D reconstruction of triangle mesh to estimate the volume of the chamber of tomb 3. The point spacing is ca. 5 cm.

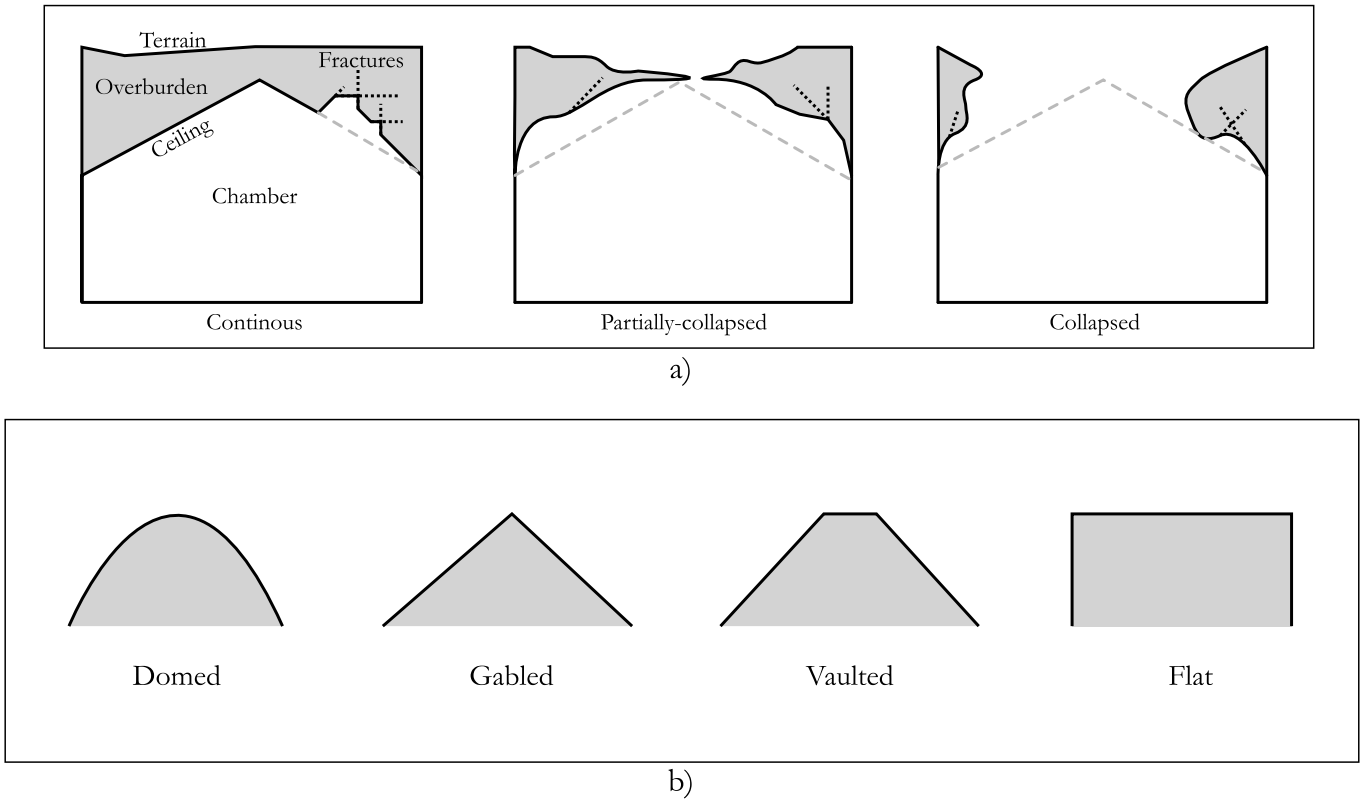

Fig. 8. Illustration of categories followed to describe the degree of preservation of chamber overburden (a) and the observed type of ceiling (b). When an observed geometry does not match with one of the defined categories in (b), the ceiling type is declared as "Not Defined (N)".

polygonal.

Accessory elements: Number of architectural accessories such as side chambers, pits, and niches identified in the tombs.

The georeferenced point clouds were plotted on maps to measure and analyse the elevation and the aspect of the terrain as well as trends observed in the tombs' distribution and orientation. This involved importing the point clouds into a Geographic Information System (GIS) database within ArcGIS Desktop (ESRI, 2020).

3. Results

The resulting Mycenaean tomb catalogue has been conceptually conceived to digitally characterise the present-day architecture and, in general, the state of preservation of the chamber tombs at the Aidonia cemetery. The catalogue has a graphical component consisting of thematic maps of the cemetery (Figs. 9 and 10b,c) and illustrations that showcase raw and processed point clouds depicting in detail the internal structure of each tomb (e.g., Fig. 11). A compendium encompassing all the illustrations is included in the supplementary material provided with this article. The other component consists of two tables that contain information on the geometry and the state of preservation of the chambers (Table 2) and the dromoi (Table 3). The information in the tables is arranged in ascending order following the pre-existing tomb numbering. Column headers correspond to quantitative and qualitative criteria derived from direct measurements and observations, respectively made on the TLS point clouds (see Section 2.4).

The terrain topography, the distribution of the tombs across the cemetery, and the layout of dromoi and chambers are shown in Fig. 9. Footprints of tombs occur between ca. 380 and 396 m.a.s.l (Fig. 9 a) and occupy an area of ca. 0.19 ha. In general, the tombs are uniformly distributed, though a small group (19, 2, and 3) is slightly isolated from the rest. Two tendencies are observed considering the average azimuth of the dromoi walls (Fig. 9 a; Table 3): The majority (11 tombs) are oriented northeast-southwest with an average azimuth of 16°, whereas the rest (5 tombs) are oriented northwest-southeast with an average azimuth of 345°. Given the aspect of the hillside, the terrain dips ca. 12° on average towards the south (Fig. 9 b). In general, the chamber tombs are opened to the south since they were dug in the opposite direction to the slope of the terrain. Floors of dromoi dip 12° on average towards the north, exhibiting a negative slope relative to the terrain aspect.

Tombs can be grouped by considering the structural integrity of their chamber's overburden. Most of the chambers have continuous overburdens, except for tombs 16, 17, and 20 whose overburdens completely collapsed in response to the loss of structural integrity of the natural rock formation (Table 2; Fig. 9). These tombs also exhibit poorly-preserved dromoi (Table 3). Except for tomb 16, which has a polygonal shape, chambers with partially-collapsed (tomb 1) and collapsed (tomb 17 and 20) overburden tend to be circular to semi-circular. Furthermore, tombs with such a collapse trend are located mainly on the eastern side of the cemetery (Fig. 9). In contrast, most of the tombs in the western and central cemetery exhibit chambers with continuous overburdens and tend to have a more polygonal shape. The average thickness of continuous overburdens is 2.0 m (Table 2; Fig. 9 b). When looking only at the chambers with continuous and partially-collapsed overburdens, it is possible to categorise the ceiling type of 11 tombs (Table 2): five gabled (4, 7, 8, 11, and 15), three vaulted (3, 6, and 9), two domed (1 and 5), and one flat (10). The ceiling types of five tombs (2, 16, 17, 19, and 20) were declared as "Not Defined".

The average length of chambers and dromoi is 4.9 m and 7.8 m, respectively (Tables 2 and 3). When combining both chambers and dromoi, the total length averages 12.7 m. Tomb 9 is the longest (20.5 m) and is the least symmetric since it has the lowest chamber/dromos length ratio (1:2.6) (Fig. 10 a). On the other hand, tomb 17 is the shortest (7 m) and the most symmetric (almost 1:1) tomb. Based on the area of the floor and the volume of the chamber, the tomb size can be classified as small, medium, or large. Although the chamber floor of

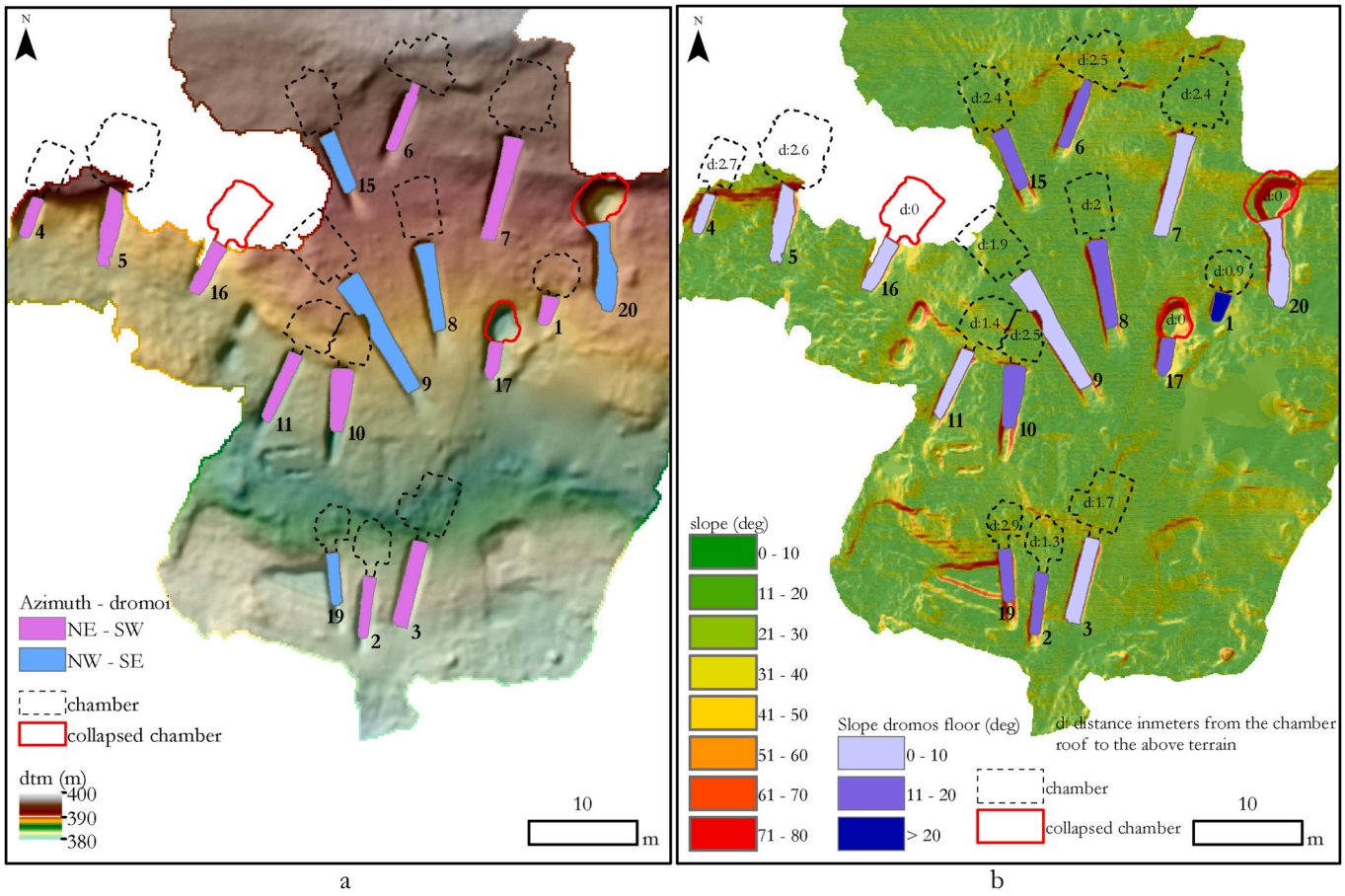

Fig. 9. Chamber tomb orientations and cemetery terrain morphology. Raster and vector data derived from the point cloud GIS-database within ArcGIS Desktop. Tomb footprints correspond to horizontal slices at the height of the sensor. a) Digital terrain model (DTM) of the cemetery setting, tomb footprints, and tomb orientation based on dromoi azimuths. Two orientation trends are observed: northeast-southwest (pink dromos) and northwest-southeast (blue dromos). b) Slope terrain map along with tomb layout and thickness of the overburden material of the chamber roofs. The terrain dips ~12° towards the south, whereas the floor of the dromoi dips 11° on average in the opposite direction. Based on the slope of the dromos floor, tomb entrances are classified as gentle (0° to 10°), moderate (11° to 20°), or steep (>20°). (For interpretation of the references to colour in this figure legend, the reader is referred to the Web version of this article.)

tomb 9 exhibits the largest area (25.2 m^2; Fig. 10 b; Table 2), tomb 5 has the chamber with the greatest volume (85.6 m^3; Fig. 10 c; Table 2). Tomb 17 has the chamber with the smallest area (5.4 m^2; Fig. 10 b). However, since its volume could not be estimated due to the absence of chamber overburden, the metric is incomplete. Therefore, with an area of 8.6 m^2 (Fig. 10 b) and a volume of 17.31 m^3 (Fig. 10 c), tomb 19 is ranked as the tomb with the smallest chamber.

Tomb 3 (Fig. 11) is used as an example of how to read the catalogue by integrating the information provided in the tables with metrics (Tables 2 and 3) and the illustrations (Figs. 9 and 10, and supplementary material). The tomb is located in the southernmost part of the cemetery, and like most tombs, tomb 3 has an orientation of northeast-southwest with an average azimuth of 14° measured in its well-preserved dromos. The chamber has a volume of ca. 54 m^3 including a west side chamber; both chambers exhibit a polygonal shape. A continuous roof covers the main chamber with an overburden of 1.7 m thick. The vaulted ceiling is 3 m high measured from the chamber floor, which occupies an area of 22.3 m^2. The tomb can be accessed through its ca. 8 m length dromos whose floor dips 9° towards the north until joining the monumental façade of the stomion where the dromos is 3.4 m high.

4. Discussion

In this chapter, the applied methods and obtained results will be briefly discussed in the following two sections: i) TLS and photogrammetric 3D documentation; and ii) Tomb segmentation challenges.

4.1. TLS and photogrammetric 3D documentation

To our knowledge, only two digital catalogues of LBA Mycenaean tombs located in the central Greek Aegean have been generated by 3D surveying techniques: one by employing TLS (this article) and one by employing photogrammetry (Turner, 2020). In this study, photogrammetry was also used to model the chamber of tomb 9. However, poor lighting conditions within the chamber hindered the effectiveness of photogrammetry. Although field photo acquisition was efficient, post-processing necessitated multiple attempts before achieving a satisfactory model. The final model had to be re-scaled to accurately represent the chamber's actual dimensions. The modelling was computationally-taxing, taking ca. three hours to generate a point cloud model of 59 million points and derive a textured colour model of 1.3 million faces from 83 photos. On the other hand, for the same chamber, TLS took less than 30 min to collect a single scan position that generated a 3D model of ~143 million points with real-world dimensions, although without coloured attributes. As an active sensor, the TLS scanner can acquire data in darkness. However, the TLS method requires an expensive and bulky sensor (in this study, 13 kg without including additional equipment such as tripods). An intermediate alternative that might fit archaeological field recording is a handheld scanner (Sirmacek et al., 2016), though the resolution and quality of data will be reduced substantially given today's technology.

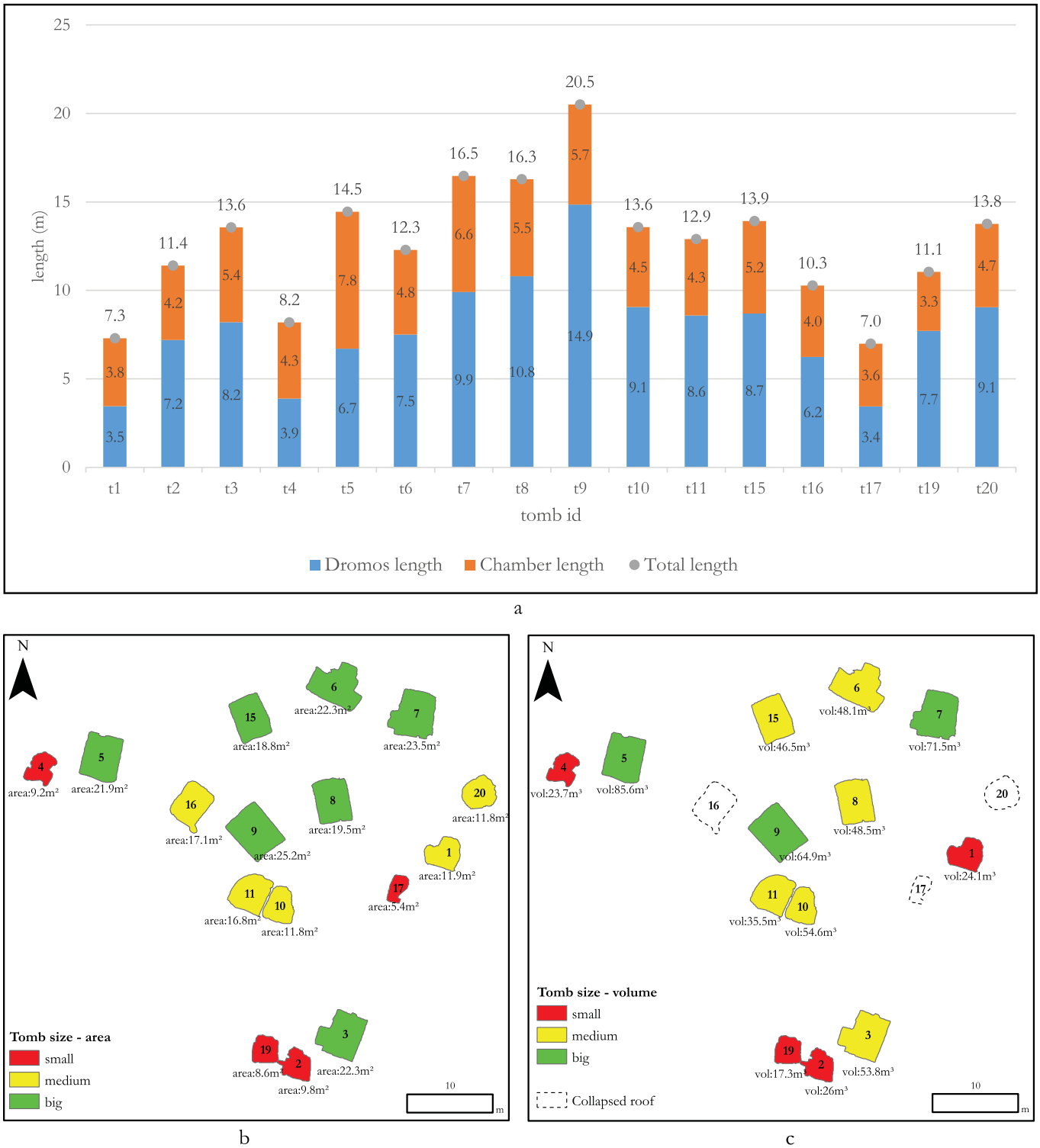

Fig. 10. Tomb measurements. a) Chart depicting the length of the tombs. b) Tomb size based on the area of the floor of the chambers. c) Tomb size based on the volume of the chamber. Tomb footprints in b) and c) correspond to the horizontal slice at the level of the chamber floor.

4.2. Tomb segmentation challenges

The segmentation of the point clouds facilitated the dissection of tomb architectural elements for analysis. However, with the employed method, the segmentation process was not straightforward given the complexity of tomb surface geometries. Architectural elements of tombs exhibit irregular surfaces (e.g., varying from non-planar to planar), and, in general, the inherent surface roughness hinder the effectiveness of the method. Therefore, the process required trial and error until a suitable parameterisation that applied for most of the tombs was found. In order to reduce inconsistencies when estimating normal vectors from the undulating surfaces and to reduce the computational time, the point clouds had to be down-sampled to 0.05 m. It means that the segmented clouds deliver a lower resolution. If particular segments are required with higher resolution, bounding polygons that envelope the down-sampled versions can be generated and used to extract the desired segments

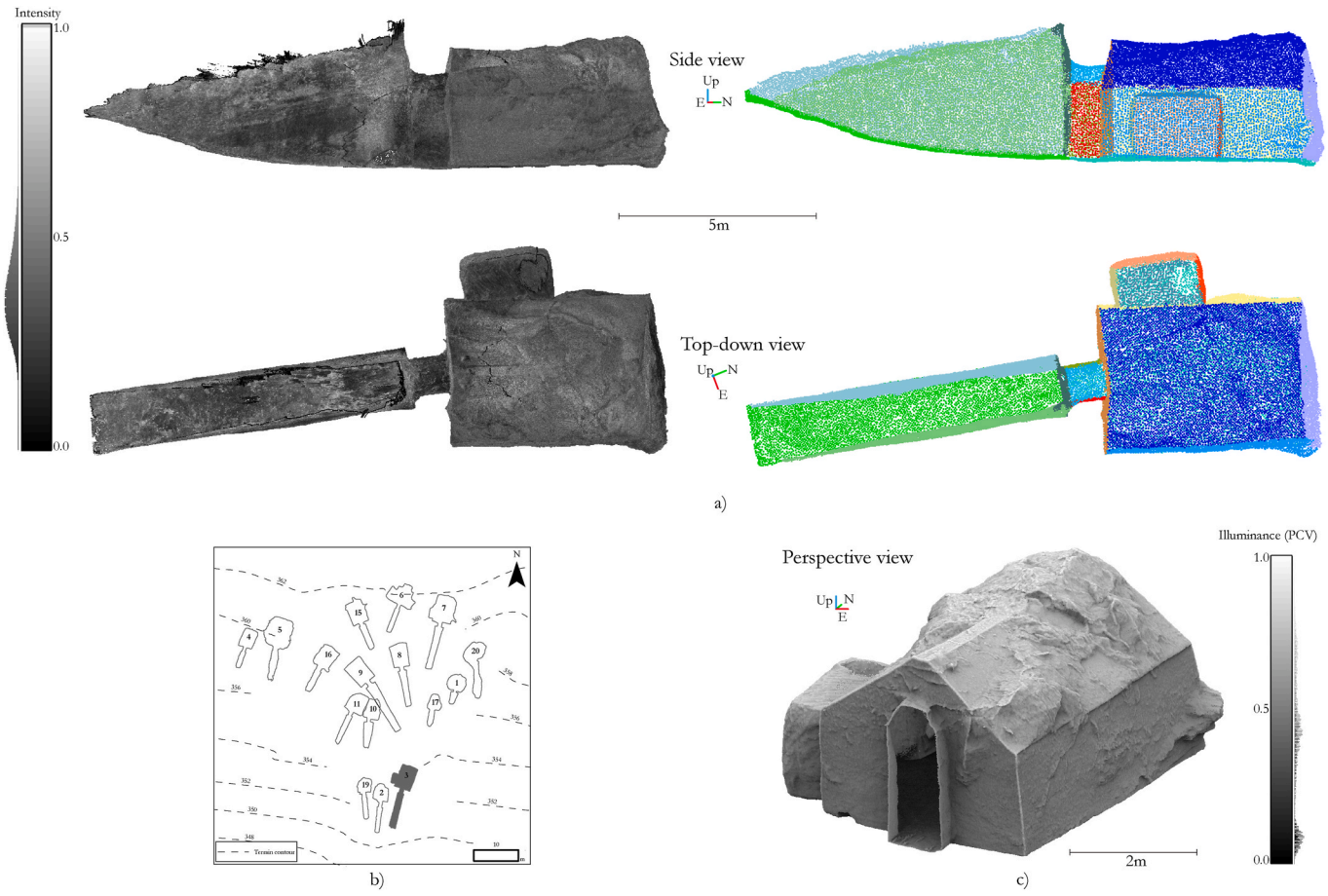

Fig. 11. Tomb 3. a) Left: Raw point cloud with point spacing of ~0.7 mm displayed using intensity. Right: Processed point cloud with point spacing of ~0.05 m coloured by segment ID. b) Plan view of cemetery setting and tomb footprints, where the position of tomb 3 is highlighted in grey. Tomb footprints correspond to the horizontal slices at the height of the sensor. c) Perspective view of the chamber of tomb 3. Point cloud visualization using calculated illuminance (Portion de Ciel Visible (PCV); Tarini et al. (2003)).

Table 2
Dimensional survey: Measurements and observations of individual chambers made directly from TLS point clouds.

TombID	[a]OI	Ceiling type	[b]Shape	Side chamber	Pit	Niche	[c]H×W×L (m)	[d]Area (m^2)	Volume (m^3)	[e]OT (m)
1	+-	D	C	NE	1	NE	2.2×4.2×3.8	11.9	24.1	0.9
2	+	N	SP	NE	1	NE	2.7×3.3×4.2	9.8	26.0	1.3
3	+	V	P	1	NE	NE	3.0×3.6×5.4	22.3	53.8	1.7
4	+	G	P	NE	3	NE	2.1×3.2×4.3	9.2	23.7	2.7
5	+	D	P	NE	5	NE	2.8×6.4×7.8	21.9	85.6	2.6
6	+	V	P	3	4	NE	2.9×6.1×4.8	22.3	48.2	2.5
7	+	G	P	1	2	NE	3.0×4.7×6.6	23.5	71.5	2.4
8	+	G	P	NE	1	NE	3.1×3.7×5.5	19.5	48.6	2.0
9	+	V	P	NE	1	NE	3.3×4.2×5.7	25.2	64.9	1.9
10	+	F	SP	NE	1	NE	1.8×2.9×4.5	11.8	54.6	2.5
11	+	G	SP	NE	3	NE	2.7×3.9×4.3	16.8	35.5	1.4
15	+	G	P	NE	5	2	2.7×4.0×5.2	18.8	46.5	2.4
16	–	N	P	NE	NE	NE	ND×3.7×4.0	17.1	ND	ND
17	–	N	SC	NE	NE	1	ND×2.6×3.6	5.4	ND	ND
19	+	N	SC	NE	NE	NE	2.3×3.1×3.3	8.6	17.3	2.9
20	–	N	C	NE	NE	NE	ND×3.9×4.7	11.8	ND	ND

Overburden integrity (OI): Continuous +, Partially-collapsed + -, Collapsed -
Ceiling type: Domed D, Vaulted V, Gabled G, Flat F, Not Defined N.
Chamber shape: Circular C, Semi-circular SC, Polygonal P, Semi-polygonal SP, No Data ND, No Evidence NE.

[a] OI: Overburden integrity.
[b] Shape of the chamber measured at the height of the sensor.
[c] H: height; W: width; L: length.
[d] Area of the chamber floor.
[e] OT: Overburden thickness.

Table 3
Dimensional survey: Measurements and observations of individual dromoi made directly from TLS point clouds.

TombID	Wall integrity	[a]Azimuth (°)	[b]Dip (°)	Height Stomion (m)	[c]Length (m)	Dip Floor (°)	Dip Terrain (°)	[d]Angle BTF (°)
1	++	16	81	2.0	3.5	22	14	36
2	++	7	84	3.5	7.2	15	14	29
3	++	14	85	3.4	8.2	9	17	25
4	+	19	87	2.1	3.9	8	23	31
5	–	12	58	ND	6.7	3	11	14
6	+	21	87	3.7	7.5	13	20	33
7	++	14	80	3.9	9.9	8	18	26
8	++	349	86	3.9	10.8	12	11	23
9	+	329	80	4.1	14.9	8	11	19
10	++	6	78	3.3	9.1	11	11	22
11	++	25	83	2.7	8.6	7	14	21
15	++	337	82	3.3	8.7	15	14	29
16	–	27	61	ND	6.2	6	14	19
17	–	14	64	ND	3.4	16	11	24
19	++	355	85	3.8	7.7	17	15	32
20	–	355	79	ND	9.1	8	12	18

Wall integrity: Well-preserved ++,
No Data ND, Fairly-preserved +, Poorly-preserved -
[a] Average azimuth of dromos walls.
[b] Average dip of dromos walls.
[c] Length of the dromos measured in the floor.
[d] Acute angle between the floor of the dromos and the terrain above.

from a higher-resolution cloud. The bounding polygons can be obtained using, e.g., the alpha shape approach (Edelsbrunner et al., 1983).

5. Conclusions and recommendations

Through the generation of the digital tomb catalogue of the middle cemetery of Aidonia, this study demonstrates a successful integration of TLS technique combined with geosciences in the permanent documentation of an endangered cultural heritage site. A high resolution and accuracy 3D model of TLS-derived point clouds with millimetre resolution was generated to produce the catalogue. The model resulted from the integration of 51 georeferenced scan positions representing the architecture of 16 chamber tombs and the cemetery terrain, which dips ca. 12° towards the south. The applied tomb segmentation enabled measuring with high accuracy the dimensions and orientations of tomb architectural elements. The chamber tombs are mainly orientated northeast-southwest and northwest-southeast, and average 12 m in length from the beginning of the dromos to the end of the chamber. 208 (13 variables across 16 tombs) architectural and geological measurements, and 112 (7 variables across 16 tombs) qualitative observations were made directly from the clouds to generate the catalogue. The chamber overburdens of 3 out of 18 tombs have completely collapsed, and therefore the volumes of these chambers could not be estimated. The average volume of those chambers that still preserve their roofs is 46 m^3.

Future work aims to maximise the use of the acquired dataset and gather additional TLS surveys to provide informed decisions for site preservation and explore undiscovered tombs. Periodic TLS surveys facilitate temporal model comparisons to track induced natural and anthropogenic changes over time; it is recommended that more TLS surveys are collected in the area at a cost-efficient interval. Efforts are needed to map the anthropogenic linear features such as chisel marks observed in the tombs surfaces. Likewise, natural features (e.g., fractures and bedding plane) can be mapped across the tombs and eventually provide hints about the tombs' structural integrity. By leveraging the high-quality dataset, implementing machine learning can enhance information extraction and automate mapping processes. Conducting near surface geophysical studies at the site, such as ground penetrating radar (GPR), electrical resistivity tomography (ERT), and seismic refraction tomography, is recommended for generating holistic 3D models that integrate the archaeological and topographic information from the surface with potential geophysical anomalies that suggest new tomb discoveries. The TLS dataset and the digital catalogue of the Aidonia cemetery are now part of the legacy of the Aegean cultural heritage. They are available for society in general and future generations. To enhance research and promote education and outreach, augmented reality platforms and virtual reality museum exhibitions that showcase 3D models of chamber tombs are recommended.

CRediT authorship contribution statement

Ivan Gutierrez: Writing – original draft, Visualization, Software, Project administration, Methodology, Investigation, Data curation, Conceptualization. **Roderik Lindenbergh:** Writing – review & editing, Visualization, Supervision, Software, Resources, Conceptualization. **Lisa Watson:** Writing – review & editing, Supervision, Resources, Funding acquisition, Conceptualization. **Kim Shelton:** Writing – review & editing, Supervision, Resources.

Declaration of competing interest

The authors declare that they have no known competing financial interests or personal relationships that could have appeared to influence the work reported in this paper.

Acknowledgements

This work was funded by the Ministry of Education and Research, Norway. The authors acknowledge the invaluable cooperation provided by Timo Bisschop and Sylwia Wasilewska on the data collection. We thank anonymous reviewers for their helpful input.

Appendix A. Supplementary data

Supplementary data to this article can be found online at https://doi.org/10.1016/j.daach.2024.e00319.

References

Allmendinger, R.W., Cardozo, N., Fisher, D.M., 2011. Structural Geology Algorithms: Vectors and Tensors. Cambridge University Press.
ASF DAAC, 2015. ALOS PALSAR Radiometric Terrain Corrected High Res; Includes Material © JAXA/METI 2007. ASF DAAC. https://doi.org/10.5067/Z97HFCNKR6VA accessed: 2019-11-11. https://asf.alaska.edu/III-1/143/2016/.

Axelsson, P., 2000. Dem generation from laser scanner data using adaptive tin models. International archives of photogrammetry and remote sensing 33 (4), 110–117.
Besl, P.J., Jain, R.C., 1988. Segmentation through variable-order surface fitting. IEEE Trans. Pattern Anal. Mach. Intell. 10 (2), 167–192.
Besl, P.J., McKay, N.D., 1992. Method for registration of 3-d shapes. *Sensor fusion IV: control paradigms and data structures*. Spiegel 1611, 586–606.
Böhler, W., Marbs, A., 2002. 3d Scanning Instruments–Cipa. *Heritage. Documentation-International Workshop on Scanning for Cultural Heritage RecordingCorfu, Greece–2002*.
Bolles, R.C., Fischler, M.A., 1981. A ransac-based approach to model fitting and its application to finding cylinders in range data. *IJCAI*. Citeseer 1981, 637–643.
Brodu, N., Lague, D., 2012. 3d terrestrial lidar data classification of complex natural scenes using a multi-scale dimensionality criterion: applications in geomorphology. ISPRS J. Photogrammetry Remote Sens. 68, 121–134.
Casselmann, C., Fuchs, M., Ittameier, D., Maran, J., Wagner, G.A., 2004. Interdisziplinäre landschaftsarchäologische forschungen im becken von phlious, 1998-2002. Archäologischer Anz. (1), 1–57.
Cavanagh, W.G., Mee, C., 1998. A Private Place: Death in Prehistoric Greece, vol. 125. Coronet Books Incorporated.
Cline, E.H., 2010. The Oxford Handbook of the Bronze Age Aegean. Oxford University Press.
Conrad, O., Coauthors, 2015. System for automated geoscientific analyses (SAGA) v. 2.1.4. Geosci. Model Dev. (GMD) 8 (7), 1991–2007. https://doi.org/10.5194/gmd-8-1991-2015, 10.5194/gmd-8-1991-2015.
Demakopoulou, K., 1998a. The Aidonia Treasure. Seals and Jewellery of the Aegean Late Bronze Age. Archaeological Receipts Fund Publications Department, Athens.
Demakopoulou, K., 1998b. The return of the "mycenaean Treasure" to Greece. In: Demakopoulou, Katie (Ed.), The Aidonia Treasure. Seals and Jewellery of the Aegean Late Bronze Age. Archaeological Receipts Fund Publications Department, Athens, pp. 17–20.
Edelsbrunner, H., Kirkpatrick, D., Seidel, R., 1983. On the shape of a set of points in the plane. IEEE Trans. Inf. Theor. 29 (4), 551–559.
ESRI, 2020. ArcGIS Desktop (*Version 10.8*) *[Computer software]*.
Evans, J.S., Hudak, A.T., 2007. A multiscale curvature algorithm for classifying discrete return lidar in forested environments. IEEE Trans. Geosci. Rem. Sens. 45 (4), 1029–1038.
Fuchs, M., Lang, A., Wagner, G.A., 2004. The history of holocene soil erosion in the phlious basin, ne peloponnese, Greece, based on optical dating. Holocene 14 (3), 334–345.
Galanakis, Y., 2018. A survey of late bronze age funerary archaeology over the last 25 years in the central and southern aegean. Archaeol. Rep. 64, 85–101.
Girardeau-Montaut, D., 2016. CloudCompare [GPL software]. CloudCompare, accessed: 2018-08-1, version 2.11.3. http://www.cloudcompare.org.
Groshong, R.H., 2006. 3-D Structural Geology. Springer.
I.G.S.R, 1970. Geological Map of greece, Nemea Sheet. Institute of Geology and Mineral Exploration, Map. 1:50.000. Printed by K. Papachrysanthou & Co.
Karkanas, P., Dabney, M.K., Smith, R.A.K., Wright, J.C., 2012. The geoarchaeology of mycenaean chamber tombs. J. Archaeol. Sci. 39 (8), 2722–2732.
Kaza-Papageorgiou, K., 1998. Finds from the excavation of the mycenaean cemetery at aidonia 1978-1980: pottery, figurines, seals and jewellery. In: Demakopoulou, Katie (Ed.), The Aidonia Treasure. Seals and Jewellery of the Aegean Late Bronze Age. Archaeological Receipts Fund Publications Department, Athens, pp. 36–67.
Kazhdan, M., Bolitho, M., Hoppe, H., 2006. Poisson surface reconstruction. In: Proceedings of the Fourth Eurographics Symposium on Geometry Processing, vol. 7.
Krystalli-Votsi, K., 1989. Τα *δακτυλ'ιδια από τα αηδόνια* κορινθ'ιας. Φ'ιλια επη εις' Γεωργ'ιον Ε. Μυλωναν' 3, 34–43.
Krystalli-Votsi, K., 1998. The excavation of mycenaean cemetery at aidonia. In: Demakopoulou, Katie (Ed.), The Aidonia Treasure. Seals and Jewellery of the Aegean Late Bronze Age. Archaeological Receipts Fund Publications Department, Athens, pp. 21–31.
Krystalli-Votsi, K., Kaza-Papageorgiou, K., 2013. Το μυκηναικό νεκροταφε'ιο των Αηδονιων. In: Kissas, K., Niemeier, W.-D. (Eds.), The Corinthia and the Northeast Peloponnese: Topography and History from Prehistoric Times until the End of Antiquity. Hirmer Verlag GmbH, Munich, pp. 417–424.
Kvapil, L., Shelton, K., 2019. Among the ancestors at aidonia. *PAST AND MEMORYIN THE AEGEAN BRONZE AGE*, 293–299. In: Borgna, E., Caloi, I., Carinci, F.M., Laffineur, R. (Eds.), MNHMH/MNEME. Proceedings of the 17th International Aegean Conference. University of Udine, Department of Humanities and Cultural Heritage, Ca' Foscari University of Venice, Department of Humanities, pp. 17–21. April 2018.
Lambers, K., Remondino, F., 2008. Optical 3d measurement techniques in archaeology: recent developments and applications. In: Proceedings of the 35th International Conference on Computer Applications and Quantitative Methods in Archaeology (CAA), pp. 27–35. Berlin, Germany, April 2-6, 2007.
Laserdata, 2017. LIS Pro 3D software package. https://www.laserdata.at/software.html.
Leica Geosystems, 2021. Leica ScanStation C10. Leica Geosystems, 2021-0909. https://leica-geosystems.com/products/laser-scanners/scanners.
Logan, T.A., Coauthors, 2014. Radiometrically terrain corrected ALOS PALSAR data available from the Alaska satellite facility. AGU Fall Meeting Abstracts 2014. IN33B–3762.
Mozas-Calvache, A.T., Pérez-García, J.L., Gómez-López, J.M., 2023. Geometrical study of middle kingdom funerary complexes in qubbet el-hawa (aswan, Egypt) based on 3d models. Virtual Archaeology Review 14 (28), 1–18.
Nguyen, A., Le, B., 2013. 3d point cloud segmentation: a survey. *2013 6th IEEE conference on robotics, automation and mechatronics (RAM)*. IEEE 225–230.
Paraskevopoulos, S., 1990. Rilevamento e sedimentologia del bacino dell' argolide, pliopleistocene (peloponneso): zona tra stimfalia e nemea (nomos corintos). Ph.D. thesis, Università degli Studi di Bologna.
Pérez-García, J.L., Mozas-Calvache, A.T., Barba-Colmenero, V., JiménezSerrano, A., 2019. Photogrammetric studies of inaccessible sites in archaeology: case study of burial chambers in qubbet el-hawa (aswan, Egypt). J. Archaeol. Sci. 102, 1–10.
Ragan, D., 2009. Structural Geology: an Introduction to Geometrical Techniques. Cambridge University Press.
Remondino, F., 2011. Heritage recording and 3d modeling with photogrammetry and 3d scanning. Rem. Sens. 3 (6), 1104–1138.
Remondino, F., El-Hakim, S., 2006. Image-based 3d modelling: a review. Photogramm. Rec. 21 (115), 269–291.
Sapidis, N.S., Besl, P.J., 1995. Direct construction of polynomial surfaces from dense range images through region growing. ACM Trans. Graph. 14 (2), 171–200.
Shelton, K., 2020. "*You can't take It with you": the sociopolitical Context of changing burial Traditions during the palatial Period at Mycenae*. In: Death in Late Bronze Age Greece: Variations on a Theme. Oxford University Press, pp. 56–57. https://doi.org/10.1093/oso/9780190926069.003.0003.
Sirmacek, B., Shen, Y., Lindenbergh, R., Zlatanova, S., Diakite, A., 2016. Comparison of Zeb1 and Leica C10 indoor laser scanning point clouds. ISPRS Annals of the Photogrammetry, Remote Sensing and Spatial Information Sciences III-1, 143–149, 10.5194/isprs-annals-III-1-143-2016. https://www.isprs-ann-photogramm-remote-sens-spatial-inf-sci.net/III-1/143/2016/.
Slane, K.W., 2017. Tombs, Burials, and Commemoration in Corinth's Northern Cemetery, vol. 21. ISD LLC.
Tarini, M., Cignoni, P., Scopigno, R., 2003. Visibility Based Methods and Assessment for Detail-Recovery. IEEE Visualization, 2003. VIS 2003., IEEE, pp. 457–464.
Touchais, G., 1987. Chronique des fouilles et découvertes archéologiques en grèce en 1986. Bull. Corresp. Hell. 111, 519–583. URL. https://www.persee.fr/doc/bch_0007-4217_1987_num_111_2_6805.
Turner, D.R., 2020. Comparing Mycenaean Tomb Building with Energetics and Memory. Ph.D. thesis, Universiteit Leiden.
Vieira, M., Shimada, K., 2005. Surface mesh segmentation and smooth surface extraction through region growing. Comput. Aided Geomet. Des. 22 (8), 771–792.
Vosselman, G., 2013. Point cloud segmentation for urban scene classification. Int. Arch. Photogram. Rem. Sens. Spatial Inf. Sci. 1 (257–262), 1.
Vosselman, G., Maas, H.-G., 2010. Airborne and Terrestrial Laser Scanning. CRC press.
Weeks, K.R., 2010. The Theban Mapping Project's Online Image Database of the Valley of the Kings. Offerings to the Discerning Eye. Brill, pp. 333–338.
Weinmann, M., Jutzi, B., Mallet, C., Weinmann, M., 2017. Geometric features and their relevance for 3d point cloud classification. ISPRS Annals of the Photogrammetry, Remote Sensing and Spatial Information Sciences IV-1/W1, 157–164, 10.5194/isprs-annals-IV-1-W1-157-2017. https://isprs-annals.copernicus.org/articles/IV-1-W1/157/2017/.
Wichmann, V., Strauhal, T., Fey, C., Perzlmaier, S., 2019. Derivation of spaceresolved normal joint spacing and in situ block size distribution data from terrestrial lidar point clouds in a rugged alpine relief (kühtai, Austria). Bull. Eng. Geol. Environ. 78 (6), 4465–4478.
Wright, J.C., 2004. 9. comparative settlement patterns during the bronze age in the northeastern peloponnesos, Greece. Side-by-side Survey: Comparative Regional Studies in the Mediterranean World 50, 114.
Zhang, W., Qi, J., Wan, P., Wang, H., Xie, D., Wang, X., Yan, G., 2016. An easy-to-use airborne lidar data filtering method based on cloth simulation. Rem. Sens. 8 (6), 501.